JACS
JOURNAL OF THE AMERICAN CHEMICAL SOCIETY

Article

pubs.acs.org/JACS

Primary Events in the Blue Light Sensor Plant Cryptochrome: Intraprotein Electron and Proton Transfer Revealed by Femtosecond Spectroscopy

Dominik Immeln,[†] Alexander Weigel,[‡] Tilman Kottke,*[,†] and J. Luis Pérez Lustres*[,‡,§]

[†]Physical and Biophysical Chemistry, Department of Chemistry, Bielefeld University, Universitätsstrasse 25, 33615 Bielefeld, Germany

[‡] Institut für Chemie, Humboldt Universität zu Berlin, Brook Taylor Strasse 2, D-12489 Berlin, Germany

[§]Research Center for Biological Chemistry and Molecular Materials (CIQUS), Department of Physical Chemistry, University of Santiago, c/Jenaro de la Fuente s/n, E-15782 Santiago, Spain

Supporting Information

ABSTRACT: Photoreceptors are chromoproteins that undergo fast conversion from dark to signaling states upon light absorption by the chromophore. The signaling state starts signal transduction in vivo and elicits a biological response. Therefore, photoreceptors are ideally suited for analysis of protein activation by time-resolved spectroscopy. We focus on plant cryptochromes which are blue light sensors regulating the development and daily rhythm of plants. The signaling state of these flavoproteins is the neutral radical of the flavin chromophore. It forms on the microsecond time scale after light absorption by the oxidized state. We apply here femtosecond broad-band transient absorption to early stages of signaling-state formation in a plant cryptochrome from the green alga *Chlamydomonas reinhardtii*. Transient spectra show (i) subpicosecond decay of flavin-stimulated emission and (ii) further decay of signal until 100 ps delay with *nearly* constant spectral shape. The first decay (i) monitors electron transfer from a nearby tryptophan to the flavin and occurs with a time constant of τ_{ET} = 0.4 ps. The second decay (ii) is analyzed by spectral decomposition and occurs with a characteristic time constant τ_1 = 31 ps. We reason that hole transport through a tryptophan triad to the protein surface and partial deprotonation of tryptophan cation radical hide behind τ_1. These processes are probably governed by vibrational cooling. Spectral decomposition is used together with anisotropy to obtain the relative orientation of flavin and the final electron donor. This narrows the number of possible electron donors down to two tryptophans. Structural analysis suggests that a set of histidines surrounding the terminal tryptophan may act as proton acceptor and thereby stabilize the radical pair on a 100 ps time scale.

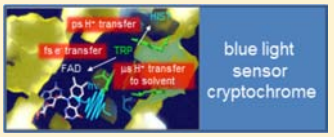

INTRODUCTION

Cryptochromes comprise a diverse family of proteins with respect to function and mechanism. The cryptochrome family includes blue light sensors that synchronize the biological clock in insects[1] and plants[2] with the external light−dark cycle and are involved in many central photoregulation processes of plant development.[3] Furthermore, cryptochromes have been demonstrated to be responsible for light-induced gene expression in diatoms[4] and bacteria[5] and for regulation of the neuronal firing rate in insects.[6] Besides their role as light sensors, insect cryptochromes have been shown to act as sensors of magnetic fields as weak as that of the Earth.[7] This finding supported previous suggestions that migratory birds might use cryptochromes to be guided by magnetic inclination.[8,9] A nonsensory function of cryptochromes is their light-independent role in the biological clock of vertebrates[10] and insects.[11] DASH cryptochromes, on the other hand, act as DNA repair enzymes[12,13] similar to the homologues of cryptochromes, the cyclobutane pyrimidine dimer (CPD), and (6−4) photolyases.[14]

Plant cryptochromes have been the subject of a series of spectroscopic studies in the recent past.[15] These blue light sensors carry an oxidized flavin adenine dinucleotide (FAD) as a chromophore.[16] FAD is noncovalently bound to the ∼500 amino acid N-terminal photolyase homology region (PHR) of the protein. The second, C-terminal domain has been shown to act as effector of the light signal.[17] Absorption of blue light by the oxidized FAD leads to formation of a neutral radical in vitro and in vivo, which acts as a signaling state.[18,19] The reduction mechanism is currently under debate, because in vivo studies showed a prominent role of a tryptophan triad for electron transfer in *Arabidopsis* cryptochrome 1 (*At*CRY1)[20] but not in the highly homologous *Arabidopsis* cryptochrome 2 (*At*CRY2).[21] This triad is present in ∼5−15 Å distance to the flavin.[22] In vitro, the resulting tryptophan radical has been detected by UV−vis spectroscopy in its deprotonated state in the microsecond[23] and millisecond[24] time domains, decaying into a tyrosine radical. Proton transfer to flavin occurs with a time constant of 1.7 μs and is separated in time from the electron transfer, which occurs faster than 100 ns.[23] This strict decoupling of electron and proton transfer to the flavin is

Received: March 3, 2012
Published: July 9, 2012

 © 2012 American Chemical Society dx.doi.org/10.1021/ja302121z | J. Am. Chem. Soc. 2012, 134, 12536−12546

unusual and implies an activation barrier provided by the protein environment. The proton donor was proposed to be an aspartic acid close to flavin N5 (Asp396 in *At*CRY1) from results of Fourier transform infrared (FT−IR) difference spectroscopy and structural considerations.[25] This proposal was supported by deviations in UV−vis and FT−IR spectroscopic signatures[26] and redox potential[27] characteristic of the plant cryptochrome radical state as compared to other flavoprotein neutral radicals without this charged aspartate. The proton transfer clearly discriminates the photochemistry of plant from that of sensory insect cryptochromes, because the latter exclusively form the flavin anion radical without protonation.[28,29] Moreover, the in vivo oxidation state of insect cryptochrome in the dark is under debate,[28,30] whereas in plant cryptochromes the observed light-induced evolution from the oxidized flavin to the neutral radical can be linked to their function.[18,19]

The initial photoreduction of plant cryptochromes has been shown to take place in less than 100 ns.[23] Further insight into the underlying processes of this crucial activation step and concurring reactions is still missing. Other flavoproteins show fluorescence quenching by electron transfer to oxidized flavin with main components ranging from 100 fs (86%) in riboflavin binding protein[31,32] to 1.8 ps (75%) in glucose oxidase.[32] In between, CPD and (6−4) photolyases have dominant fluorescence decay components of 0.5−0.8 ps.[33] Exceptionally slow is the tyrosine → FAD electron transfer in BLUF (blue light sensors using FAD): 7 ps.[34] In insect cryptochromes,[33,35] the characteristic time constant is ∼1 ps (90% amplitude) while cryptochrome/photolyase family (CPF) homologues from the picoalga *Ostreococcus tauri*, *Ot*CPF1 and *Ot*CPF2, showed electron-transfer time constants of 390 and 590 fs, respectively.[36] Later processes in CPF proteins were interpreted as a hole transport via the tryptophan triad.[36] This interpretation was inspired by the pioneering work on the reduction of the radical state in CPD photolyase[37−39] despite the differences in oxidation states. Poor sequence homology prevents us from drawing conclusions from these results about the expected behavior of plant cryptochromes. Therefore, the photocycle of plant cryptochromes has to be traced back to earliest times with ultrafast spectroscopy.

Here, we present femtosecond broad-band transient absorption measurements on the PHR domain of the plant cryptochrome CPH1 (*Chlamydomonas* photolyase homologue 1) from the green alga *Chlamydomonas reinhardtii*. This domain has been shown to serve as a model system for spectroscopic studies[23,26,40] due to its 49% identity in sequence with the established *At*CRY1-PHR and its availability in sufficient amounts from heterologous expression in *E. coli*. Detailed analysis of the spectra reveals ultrafast electron transfer as in other members of the cryptochrome/photolyase family but also an unprecedented ultrafast proton-transfer process contributing to stabilization of the radical pair.

EXPERIMENTAL SECTION

Sample Preparation. The PHR domain (amino acids 1−504) of the *Chlamydomonas reinhardtii* cryptochrome CPH1 was expressed in *E. coli* and purified via Strep-Tactin affinity chromatography as described previously.[40] A 50 mM sodium phosphate buffer, pH 7.5, containing 20% glycerol and 100 mM NaCl was used for cell lysis and purification. D-desthiobiotin (2.5 mM) was added for elution and removed afterward by repeated ultrafiltration using an Amicon Ultra filter device with a 30 kDa cutoff (Millipore). Samples were shock frozen and kept at −80 °C. Immediately before the experiment, frozen samples were thawed and centrifuged in a table-top microcentrifuge at maximum speed for 10 min. The phosphate buffer for dilution was filtered through a 0.2 μm filter.

Pump−Probe Experiment. The femtosecond pump−supercontinuum probe (PSCP) setup has been described elsewhere.[41,42] Briefly, a femtosecond Ti:Sa oscillator/multipass amplifier laser system (Femtolasers, 500 Hz, 0.7 mJ, 800 nm, 35 fs) was used. The output of the laser system was split for second-harmonic generation and to pump a collinear parametric amplifier (Topas, Light Conversion). The output of the Topas was tuned to 445 nm, compressed with a quartz prism pair, and used for optical pumping in the absorption maximum (1 μJ, ∼100 μm spotsize). The second harmonic of the Ti:Sa fundamental (10 μJ) was used for generating a white light continuum on a CaF_2 plate mounted on an *XY* stage, which moves stepwise and in synchrony with the laser system. The continuum was spectrally filtered, split for reference, and 1:1 imaged onto the sample cell. Reference and transmitted beams were further imaged onto the entrance planes of homemade grating spectrographs. Registration was accomplished with photodiode arrays (Hamamatsu S3901Q, 512 pixels) at ∼2 nm resolution. The transient absorption signal was constructed from signal and reference spectra measured in the dark and obtained successively with the pump−probe sequence (on−off, off−on, and on−on). One hundred fifty baseline- and scattering-corrected spectra were averaged for each delay. Sample solutions were kept in a 0.5 mm thick CaF_2 cell (0.5 mm window thickness). The cell was continuously shaken in one dimension with 10 Hz frequency and 5 mm amplitude (400 μm/pump−shot). Thus, the linear rate of the cell is sufficient to replenish the sample after every pump−shot, and cell shaking provides for sample recovery (τ = 200 s).[40] For the first 2 ps, 30 independent scans of a diluted sample (absorbance (A) ≈ 0.15 at λ_{exc} = 445 nm) were averaged. Higher concentrations were used to scan the subnanosecond time window (A ≈ 0.5 at 445 nm). Ten time scans were measured with parallel ($\Delta A_{\parallel}$) and perpendicular ($\Delta A_{\perp}$) polarizations and averaged. Magic angle spectra were reconstructed from the relation $\Delta A_{magic} = ((2 \times \Delta A_{\perp} + \Delta A_{\parallel})/3)$. No filtering or smoothing procedures were applied. The average cross-correlation over the full spectral window was 90 fs. Nonresonant solvent contribution was not subtracted. Concentration was kept as low as possible to minimize aggregation and adsorption on cell surfaces while still achieving reasonable signal amplitude. Measurements were conducted on six different samples obtained from two different batches. Results were comparable within experimental accuracy. No photodegradation nor accumulation of the long-lived neutral radical state was observed. Thus, formation of a long-lived neutral radical seems to proceed with low yield in CPH1-PHR, less than 10%, which eases sample refreshment. For AtCRY1, a similarly low yield of ∼2% was determined by transient absorption.[24]

Methods of Analysis. Transient spectra were analyzed by two methods. First, convoluted exponential and damped oscillatory functions were used to characterize the fastest stages (delays shorter than 2 ps). Second, a basis set of species-associated spectra (SAS) was defined for longer delays. For each delay, the corresponding transient spectrum $S(\lambda,t)$ is described as the product of the basis-set matrix $\mathbb{P}(\lambda)$ and the concentrations column vector $c(t)$. The equation $S(\lambda,t) = \mathbb{P}(\lambda)\cdot c(t)$ is solved in the least-squares sense, i.e., by minimizing norm $|S(\lambda,t) - \mathbb{P}(\lambda)\cdot c(t)|$. The time-dependent concentrations are obtained via the Moore−Penrose pseudoinverse matrix $c(t)$ = pinv $[\mathbb{P}(\lambda)]\cdot S(\lambda,t)$, where $\mathbb{P}(\lambda)$ is full rank. Parallel-polarization spectra were analyzed by both methods.

Model Spectra for Analysis of Picosecond Evolution. Model spectra of the species participating in photoinduced excited-state reactions of FAD in the protein environment are presented in the Supporting Information. The model spectra build the SAS matrix $\mathbb{P}$, which is used to explain spectral evolution measured with parallel polarization in the 800 ps time window. In the following we outline the methods by which the spectral shapes and molar absorption coefficients of the different species were estimated. A more extensive account is given in the Supporting Information, where the issue of spectral polarization is briefly discussed.

The excited-state (S_1) spectrum of FAD was calculated from transient absorption spectroscopy of riboflavin in solution. Spectra measured with parallel polarization in neutral water at 2 ps delay were used.[43,44] The molar extinction coefficient of S_1 was estimated by bleach subtraction. The ground-state absorption spectrum of riboflavin in neutral water was chosen for this purpose, as explained in the Supporting Information.

The difference spectrum of the flavin anion radical of CPH1-PHR was determined in the D393C mutant after blue light illumination (Hense, A.; Kottke, T. Unpublished results). For the flavin neutral radical the difference spectrum was measured in wild-type CPH1-PHR, where the neutral radical forms in microseconds[40] (see Supporting Information). The molar extinction coefficients of FAD anion and neutral radical were estimated from pulse radiolysis spectra published by Land and Swallow.[45] Radical spectra measured in other proteins[28,46] were also tested.

The spectrum of the triplet excited state of flavin in CPH1 was modeled by that of the phototropin-LOV1 domain[47] and the corresponding spectrum of free flavin.[48] However, because electron transfer occurs with a 0.4 ps time constant, the contribution of the triplet state to the CPH1 transient absorption was anticipated to be undetectable.

Radical spectra of aromatic amino acids were obtained from the literature. Spectra of tryptophan cation and neutral radicals were calculated by digitization and fit with log-normal functions of spectra of Solar et al. in water (see Supporting Information)[49] because tryptophan radical spectra in the protein environment are not available over a broad spectral window. The different environment and its influence on band positions of the tryptophan radicals might introduce some ambiguity in the fit. Tyrosyl radicals were approached in the same way[50] but do not make any contribution to the transient spectra of CPH1.

Structural Modeling. The program MODELER 9v7 was used to generate model structures. FAD was included for optimization. For the CPH1-PHR domain, the crystal structure of *At*CRY1-PHR was used as a template (PDB code 1U3C).[22] The primary sequence of the two domains shows 49% identity and 75% homology. For *Ot*CPF1, the structure of *Drosophila* (6–4) photolyase was chosen (PDB code 2WQ7),[51] whereas for *Ot*CPF2, the structure of *Arabidopsis* cryptochrome 3 was used (PDB code 2J4D).[52]

RESULTS

Transient absorption spectra of the PHR domain of plant cryptochrome CPH1 were recorded for delay times ranging from 0.15 to 800 ps. The time range of 0.15–1.5 ps was analyzed first (Figure 1). The transient spectra with parallel pump–probe polarization show the negative contributions of bleach and stimulated emission (SE) with maxima at 450 and 555 nm, respectively. The bleach contribution can be directly compared to a representative absorption spectrum of the sample (yellow-filled curve). Strong excited-state absorption (ESA) was observed at 370 nm together with a weak ESA feature at 515 nm. The earliest spectrum, measured directly after the coherent contribution, is comparable to that obtained for riboflavin[43] and (FAD)[44] in water. In all these spectra the SE band is about two times weaker than the bleach. After 2 ps, SE decayed almost completely but bleach and ESA in the UV remained nearly constant during the same period. We note at this stage that the time evolution of the UV ESA band (~370 nm) monitors the falling edge of the coherent contribution. This is due to the longer pump–probe cross correlation in the UV and is not directly associated to spectral or population dynamics. Broadly similar behavior was described by Brazard et al. in their femtosecond study of the *Ot*CPF1 and *Ot*CPF2 proteins[36] and assigned to electron transfer. In contrast, transient absorption of FAD in water decays with a major component of 6.5 ps[44,53] with constant spectral shape, i.e.,

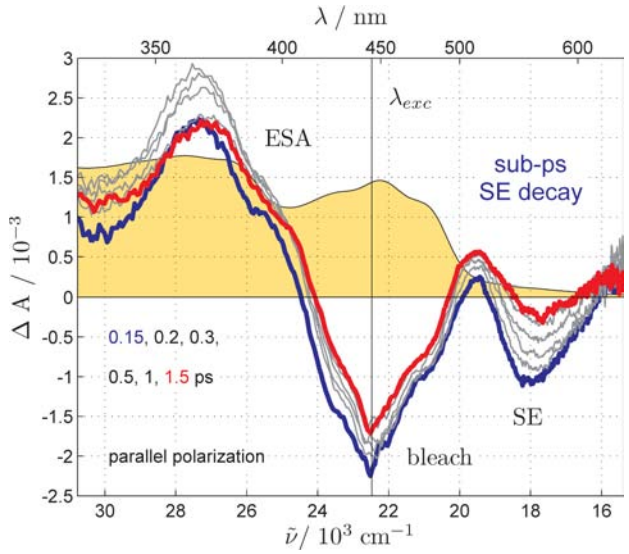

Figure 1. Subpicosecond broad-band transient absorption spectra of cryptochrome measured with 445 nm excitation and parallel pump–probe polarization at the indicated delay times. Spectra obtained at 0.15 (blue) and 1.5 ps (red) are shown in color, while gray lines correspond to intermediate delays. Bleach, ESA, and SE indicate the bleach, excited-state absorption, and stimulated emission contributions, respectively. Yellow-filled curve shows a scaled steady-state absorption spectrum of the sample. Horizontal black line marks the zero level of signal, whereas the vertical line indicates the position of the excitation pulse. Rapid decay of stimulated emission is observed.

transient species do not accumulate. Thus, subpicosecond decay of flavin SE indicates electron transfer from an aromatic rest in the protein pocket.

The spectral evolution on the picosecond time scale is shown in Figure 2 for magic angle polarization. A clear decay of the ESA band in the UV was observed between 10 and 100 ps delay (Figure 2A). The red wing of the spectrum evolves in the same time scale: ESA bands at 515 and ~625 nm decayed, while bleach and signal at 555 nm stayed practically constant. Between 100 and 800 ps (Figure 2B) the signal decayed slowly at essentially constant spectral shape. Since magic angle polarization was used, the slow decay originates from a change in concentration of the involved species on the picosecond to nanosecond time scale.

The time-resolved anisotropy is shown in Figure 3 for selected probe wavelengths. The anisotropy (r) was calculated from transient absorption experiments with parallel and perpendicular polarization of the probe pulse according to the definition $r = (\Delta A_{\parallel} - \Delta A_{\perp})/(\Delta A_{\parallel} + 2\Delta A_{\perp})$. r may take values between −0.2 and 0.4 for single transitions (see Supporting Information). It reflects the difference in transient absorption observed when probing with parallel or perpendicular polarizations relative to the pump field and originates from *photoselection*. An orientational anisotropy is introduced in the excited sample by the pump field at time zero. Its analysis is a valuable means of timing orientational redistribution of molecules and/or their transition dipole moments with regard to the photoselection direction. Experiments performed with 0.006, 0.2, and 2 ps steps are shown in Figure 3. While anisotropy was extracted with substantial error because of the small signal amplitude, a clear trend is observed for all wavelengths and delay times up to 800 ps.

dx.doi.org/10.1021/ja302121z | J. Am. Chem. Soc. 2012, 134, 12536–12546

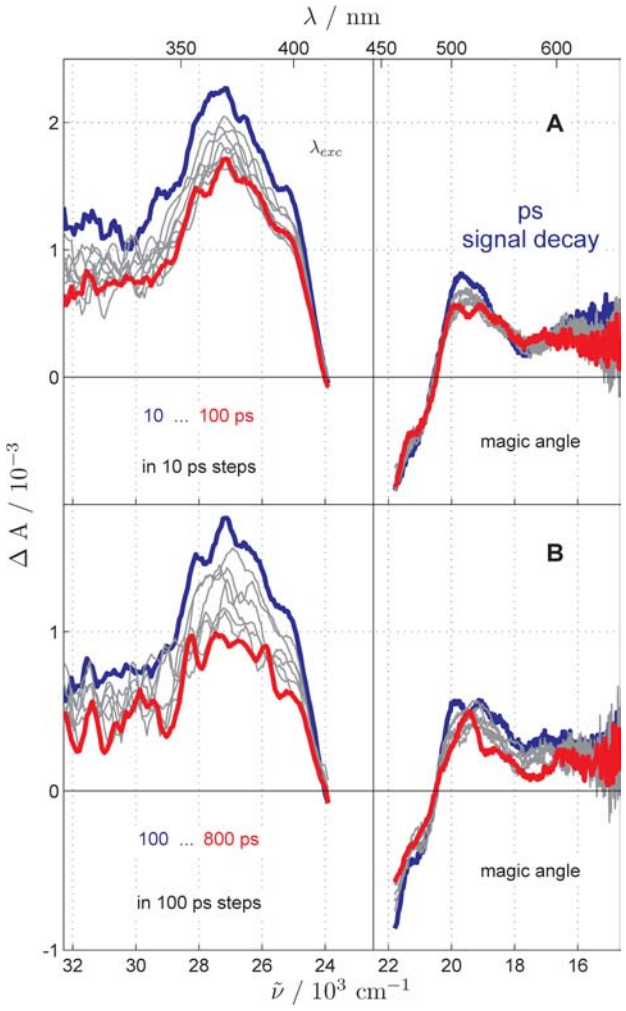

Figure 2. Picosecond broad-band transient absorption spectra of cryptochrome measured with 445 nm excitation and magic angle pump−probe polarization. (A) Spectra between 10 (blue) and 100 ps (red) in 10 ps steps. (B) Spectra ranging from 100 (blue) to 800 ps (red) in 100 ps steps. In the picosecond time scale, signal decays slowly with minor change of spectral shape.

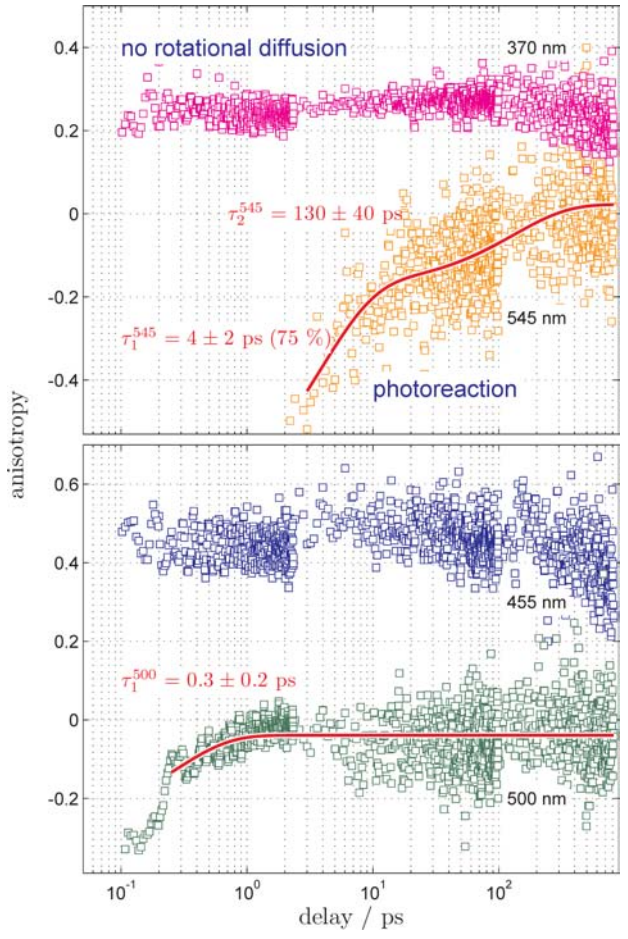

Figure 3. Time evolution of the pump−probe anisotropy during the earliest 800 ps at the indicated probe wavelengths (black labels). Anisotropy was calculated from the signals measured with perpendicular and parallel polarization for concentrated samples, ground state $A_{445\ nm} \approx 0.5$. Four representative traces are shown. Anisotropy remains constant for 455 and 370 nm, indicating that (a) the amount of free flavin (rotational time ≈ 120 ps) is negligible and (b) rotational diffusion of the protein is much slower than 800 ps. In turn, time evolution of the anisotropy at 500 and 545 nm monitors the underlying photochemical processes. Exponential fits are shown (red), and corresponding decay times, uncertainties, and contributions (in parentheses) are indicated. Anisotropy values at long delays help to identify the amino acids involved in the photoreaction.

The anisotropy stays constant at 455 and 370 nm with approximate values of 0.45 and 0.25, respectively. Values slightly above 0.4 at 455 nm may indicate a small contribution of pump scattering to the signal. These are, within experimental uncertainty, the same values as observed for riboflavin in water at early time.[43] Interestingly, the bleach band shows maximum anisotropy at 455 nm (~0.4) and stays constant for 800 ps, while the rotational time of free flavin is about 120 ps in water.[43,44] Thus, it can be concluded that (a) rotational diffusion does not take place during this time window[36] and (b) bleach and ESA do not overlap at this wavelength. Otherwise, the overlapping ESA and bleach bands would need to have parallel transition dipole moments. It is also noteworthy that the anisotropy remains constant during 800 ps for the ESA band at 370 nm. The latter indicates that the transition dipole moment of this particular FAD S_1 band is not affected by eventual electron-transfer photoreactions. This observation further confirms that rotational diffusion is much slower than 1 ns (as expected for medium-size proteins) and excludes considerable contributions from free flavin in the sample.

At 500 nm, anisotropy starts from values around −0.2 at 500 nm, which indicates that the average transition dipole is perpendicular to that of the excitation at this delay time. The signal reaches ca. −0.05 at 2 ps delay and stays constant afterward. Note that delay times before 0.2 ps were omitted because of the overwhelming amplitude of the coherent contribution between −0.15 and 0.15 ps for 500 and 545 nm. The process shows a characteristic time constant of about 0.3 ± 0.2 ps as deduced from an exponential fit. Contributions of coherent oscillations can be recognized at early times (see Discussion). The time evolution of the anisotropy at 545 nm is addressed now (Figure 3). It shows a value of −0.45 at 2 ps delay (anisotropy values outside the range from −0.2 to 0.4 are also expected for spectral regions where SE and ESA bands overlap strongly, see Supporting Information) and increases exponentially with time constants of 4 ± 2 (25%) and 130 ± 40 ps. By 100 ps delay the anisotropy is ~0, i.e., the average angle of the transition dipole of electronic transitions occurring at this

dx.doi.org/10.1021/ja302121z | J. Am. Chem. Soc. 2012, 134, 12536−12546

wavelength is about 55°. The changes in anisotropy at 500 and 545 nm over time imply that the progression of the photoreaction is directly monitored in this spectral window.

Finally, transient spectra were averaged between 100 and 600 ps delay for magic angle polarization and compared with the earliest depolarized absorption spectrum obtained for the same protein. These were acquired by streak camera experiments with nanosecond time resolution and showed mainly the presence of the flavin anion radical (Figure 4).[23] Both spectra

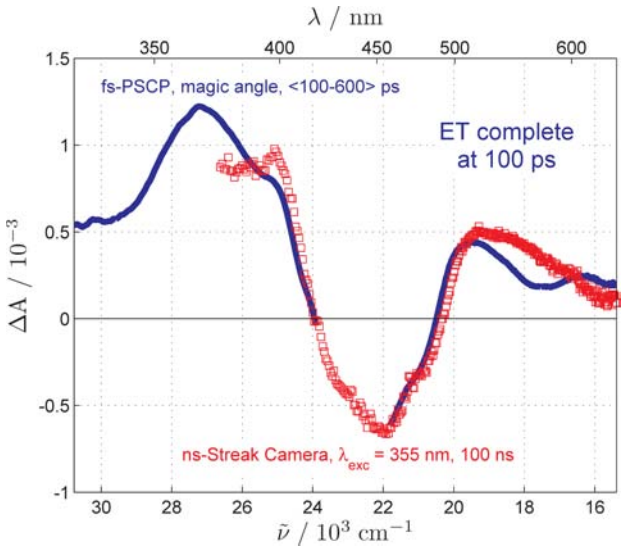

Figure 4. Pump–supercontinuum–probe spectrum (PSCP) of cryptochrome measured with magic angle polarization and averaged between 100 and 600 ps (blue). Earliest depolarized spectrum obtained by nanosecond flash-photolysis experiments with excitation at 355 nm is shown in red.[23] Small differences around 550 nm are due to the stimulated emission contribution of the flavin still present in the subnanosecond time scale.

are in fairly good agreement, especially if one considers that small deviations around 550 nm arise from the negative SE contribution still present in the femtosecond experiment. The latter points to a substantial fraction (~20–30%) of *bound* flavin with a long excited-state lifetime. Further deviations at λ_{probe} < 400 nm may be caused by the long-pass filter used to block scattered excitation light in the nanosecond experiment. In summary, the shape of the optical spectrum and therefore the population distribution of the intermediates remains practically constant between 100 ps and 100 ns. In other words, steady state has been reached already after 100 ps.

DISCUSSION

The advantage of the broad-band supercontinuum transient absorption spectra acquired from 300 to 700 nm in this study is the availability of a 3D data set for time-resolved spectral analysis. Most previous ultrafast studies on flavoproteins used narrow band data from fluorescence upconversion or transient absorption which can only be analyzed by kinetic but not by spectral-fitting procedures. As a prerequisite for spectral analysis, a basis set of reference spectra for the different possible species in the cryptochrome photoreaction needs to be defined. These spectra comprise not only those of flavin species but also any reasonable reaction product of amino acids such as tryptophan and tyrosine. The method of spectral analysis works reasonably well for long delays, when spectral relaxation is complete. Earlier spectra were analyzed by a global kinetic fit.

Femtosecond Electron Transfer. Spectral evolution before 2 ps shows fast decay of the stimulated emission band (Figure 1). A set of one exponential function, two damped oscillations, and an offset was used to characterize this very early process (Figure 5). The basis functions were convoluted with a Gaussian to account for the finite width of the pump–probe cross-correlation. The coherent spike was modeled as a sum of a Gaussian function and its first four time derivatives. The resulting cross-correlation full-width at half-maximum is 87 fs, which defines the time resolution of the experiment. The

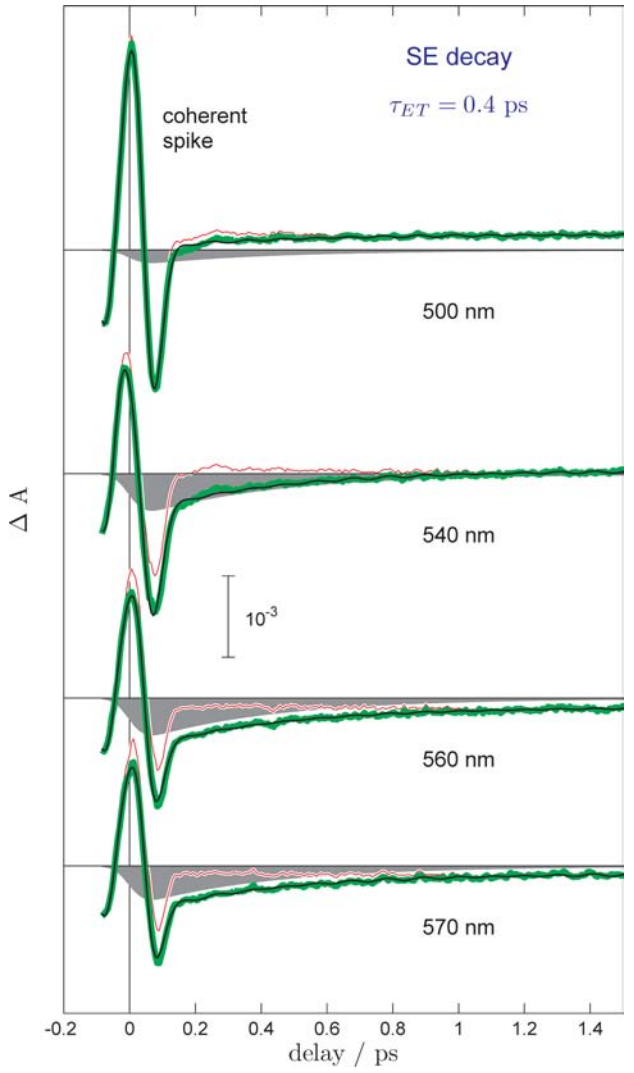

Figure 5. Global fit of transient absorption spectra in the subpicosecond region. Experimental time traces are shown in green, while black solid lines represent the fit function. One exponential and two damped oscillations were convoluted with a Gaussian instrument response function and fitted to the data. Model for the coherent spike was included together with an offset. The latter accounts for the nondecaying component in the subpicoseconds range. The gray-shadowed area represents the contribution of the exponential part. The red line shows the remaining signal after subtracting the exponential part. fwhm of the pump–probe cross-correlation was found to be 87 fs. Amplitude of the transient absorption signal is given by the inner gauge. τ_{ET} = 0.4 ps is the characteristic time constant of the primary electron-transfer reaction in the protein pocket.

dx.doi.org/10.1021/ja302121z | J. Am. Chem. Soc. 2012, 134, 12536–12546

global fit yielded an exponential decay of 2.5 ps^{-1} and damped oscillations with frequencies of 268 and 318 cm^{-1} (Figure 5). Approximately the same frequencies showed up in the Fourier analysis of residuals if only exponential functions were considered. If four oscillations were included, the time constant decreased to 2.1 ps^{-1} and frequencies of 85, 169, 267, and 320 cm^{-1} were obtained with minor improvement of fit quality. The fitted frequencies match those observed for riboflavin in solution and are assigned to vibrational wavepackets launched by the femtosecond pulse at time zero.[43,44] The exponential decay accounts for the decrease of the strength of the stimulated emission signal and is attributed to electron transfer from the nearest protein environment to the excited flavin under formation of the flavin anion radical.[36] Similar observations also suggest subpicosecond electron transfer in insect cryptochromes[35,54] and CPF proteins.[36] We obtain a characteristic time constant τ_{ET} = 0.4 ps for intraprotein electron transfer in the plant cryptochrome CPH1.

Several aromatic amino acids may act as electron donors as suggested by the crystal structure of the PHR domain of *At*CRY1 (PDB code 1U3C).[22] A crystal structure of CPH1 is not available, but all discussed residues are conserved in the highly homologous primary sequence of CPH1 and are predicted to be located at similar positions by modeling. Three tryptophan residues are located at close edge-to-edge distance to flavin: W400 (5 Å), W385 (6 Å), and W356 (7 Å). W400 has been proposed to form a tryptophan triad together with W377 (10 Å) and W324 (15 Å).[24] The closest conserved tyrosine is Y402, located at about 6 Å to flavin. CPH1 contains an additional tyrosine which is replaced by phenylalanine (F384) at a distance of 4 Å in *At*CRY1. Several studies relate the characteristic electron-transfer rate constant to the flavin−electron donor distances deduced from flavoprotein structures.[55,56] For average distances ranging from 3 to 8 Å it has been shown that the rate constant is roughly constant up to ∼6.5 Å (with $\ln k_{ET} \approx 29$) and decreases steeply further away. Therefore, subpicosecond transfer is expected for CPH1.

To understand which of these amino acids is most probably the electron donor, individual electron-transfer rates for closest aromatic residues may be estimated. Tanaka et al.[55,56] analyzed the reaction rates as a function of the average (D_{av}) and edge-to-edge (D_s) distances found in several flavoproteins. The ionization potential of the donor (tyrosine or tryptophan) and relative orientation of donor and acceptor play a minor role. Reaction rates were estimated from average flavin fluorescence decay times measured by fluorescence upconversion. Decay times longer than 10 ps are assumed to arise from self-quenching by adenine to flavin electron transfer and were not considered. An empirical equation relating the electron-transfer rate constant to D_{av} has been proposed.[55] The equation was developed for donor−acceptor distances ranging from 3 to 8 Å. Average distances D_{av} were calculated as the average of all distances between donor and acceptor atoms in the aromatic backbones of the donor and the isoalloxazine ring. The closest donor (W400) in *At*CRY1 is located beyond the higher limit: D_{av} = 8.8 ± 2.2 Å. For such average distance an unrealistically short electron-transfer time of ∼3 fs results after the empirical equation of Tanaka et al.[55] Alternatively, a coarse estimate is obtained by linear fit of $\ln k_{ET}$ as a function of the closest donor−acceptor edge-to-edge distance: $\ln k_{ET}$ (s^{-1}) = 34.3 − 1.56D_s (Å) or $\ln k_{ET}$ (s^{-1}) = 32.4 − 1.02D_s (Å) if the value for D-amino acid oxidase−benzoate complex is excluded.[55] The linear fits predict characteristic times between 1.4 and 3 ps for W400 and much longer times for all other possible reaction partners. For instance, a reaction time of 10−70 ps would be predicted for W356, comparable to the self-quenching rate. Therefore, the characteristic electron-transfer rate in cryptochromes points to an aromatic residue sitting at $D_s \leq 5$ Å. W400 is the only aromatic amino acid in this range in *At*CRY1 besides F384 and its tyrosine counterpart in CPH1. All other possible electron donors are too far away to compete.

Finally, the role of adenine as electron donor is briefly discussed. This process was studied first by Mataga and co-workers[53] by fluorescence upconversion and revisited recently by Weigel et al. by a combination of femtosecond broad-band fluorescence upconversion, transient absorption, and stimulated Raman.[44] The intramolecular electron transfer occurs with a characteristic time of 6.5 ps for the stacked conformation in solution. In contrast to cryptochrome, free flavin decays with minor changes of spectral shape. The latter indicates that no intermediates build up in the course of the reaction and shows that the back-reaction is much faster than adenine to flavin electron transfer. This observation rebuts that of Kao et al.,[33] who reported a 30−40 ps time constant for the radical pair recombination of flavin and adenine. Hence, protein to flavin electron transfer proceeds much faster in cryptochrome while the back-reaction is slowed down at the same time. The underlying mechanism is addressed in the next section.

Results from Analysis of Picosecond Evolution. The picosecond time scale was explored first with multiexponential fits. Four time constants were identified (see Supporting Information): 0.4 ps, 4−15 ps, 30−50 ps, and 0.3−1.5 ns. The latter is obtained with poor accuracy and will not be further discussed. The 0.4 ps time was already assigned to tryptophan-to-flavin electron transfer in the protein pocket. Spectral decomposition is used to shed light on the origin of the intermediate time constants: 4−15 and 30−50 ps.

Figure 6 shows the results of the spectral decomposition achieved with the molar extinction coefficients of flavin S_0 (accounting for the bleach), flavin S_1, flavin anion radical ($Fl^{\bullet -}$), tryptophan cation radical ($WH^{\bullet +}$), and tryptophan neutral radical ($W^{\bullet}$). In line with previous studies with nanosecond time resolution,[23] extensions of the basis set to include flavin neutral radical, tyrosyl radicals, and/or flavin triplet state did not improve fit quality and led to unphysical results. Time-dependent concentrations and concentration ratios were derived by this procedure for all participating species (Figure 7). The outcome of the fit may be used to weight its soundness. First, the bleach and S_1 state of flavin are found to evolve in exactly the same way, as expected. Note that the spectrum of flavin anion radical carries its own bleach. The maximal concentration of flavin anion radical formed is $\sim 10^{-5}$ M, which is reasonable. The same order of magnitude results if the ground-state concentration of $\sim 10^{-4}$ M is multiplied by, e.g., 10% excitation efficiency and 80% electron transfer. Next, concentrations of flavin and tryptophan radicals are alike, indicating that they are partners of the same photoreaction. Finally, the concentration ratios obtained concord reasonably well with those found independently in the nanosecond and microsecond time range.[23] The fit results obtained for two different batches are the same within experimental accuracy. Interestingly, at 800 ps S_1 flavin is still present with a concentration of slightly less than 2×10^{-6} M, while that of the flavin anion radical is $\sim 6 \times 10^{-6}$ M. It implies that the initial electron-transfer step is blocked in 20−30% of the proteins. The latter indicates structural heterogeneity. Heterogeneous

dx.doi.org/10.1021/ja302121z | J. Am. Chem. Soc. 2012, 134, 12536−12546

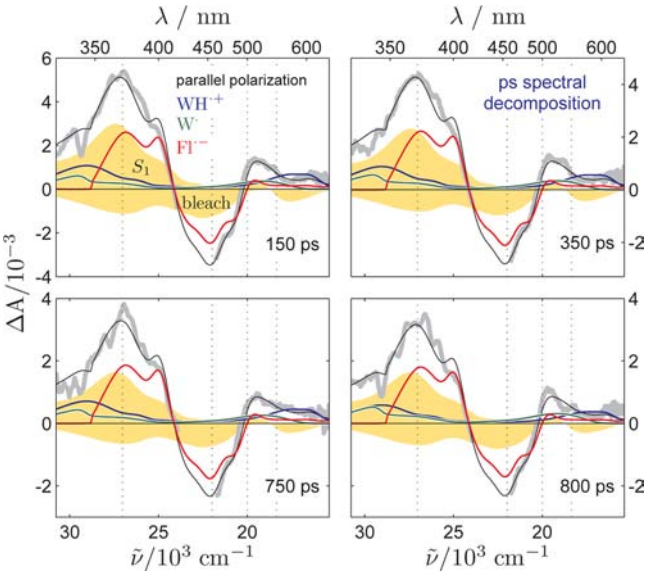

Figure 6. Spectral decomposition at selected delay times of the transient absorption (thick gray lines) recorded with parallel polarization. Molar extinction coefficients of FAD S_0 and S_1 states (negative and positive, respectively, yellow-filled spectra), FAD anion radical ($Fl^{\bullet -}$, red), tryptophan cation radical ($WH^{\bullet +}$, blue), and tryptophan neutral radical ($W^{\bullet}$, green) build up the basis set. Difference between the experiment and the best-fit linear combination of the spectral basis (thin black solid line) was minimized. Gap between 430 and 460 nm was excluded from the fit because of strong pump scattering. Horizontal black solid lines mark the zero level of signal. Vertical dotted lines mark the spectral positions at which signal anisotropy was analyzed. Note that the bleach spectrum (S_0) enters with a negative sign and therefore leads to a positive concentration in the spectral decomposition. Negative peak at ~570 nm corresponds to stimulated emission from the S_1 state.

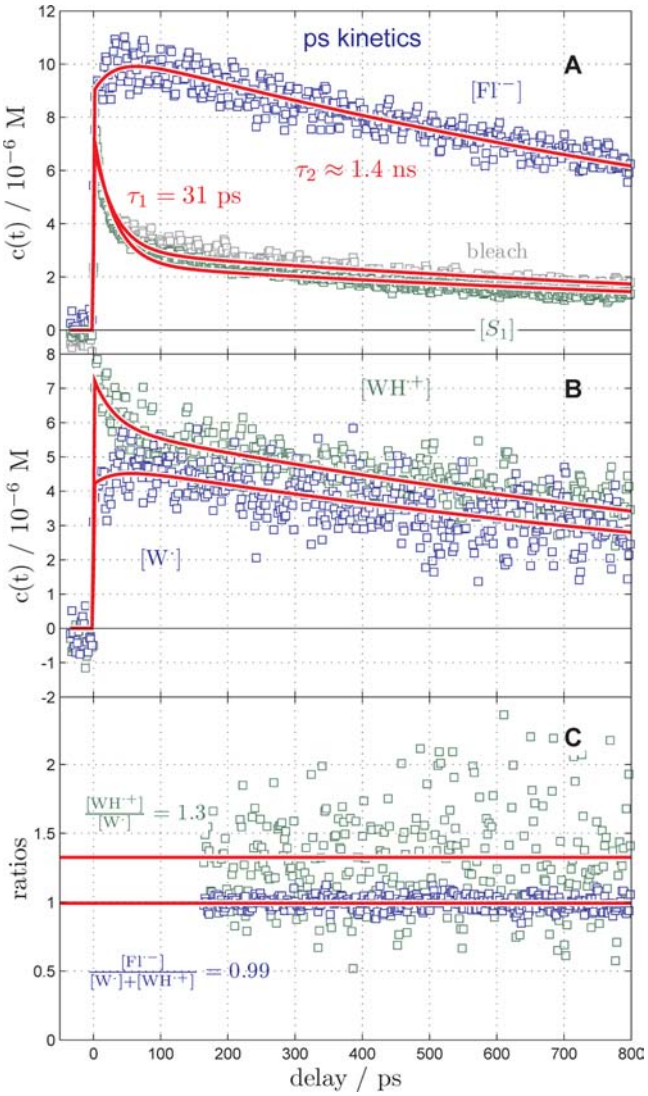

Figure 7. Analysis of time-dependent concentrations obtained from the spectral decomposition of cryptochrome transient absorption in the picosecond time scale (Figure 6). (A) Time evolution of the flavin anion radical concentration (blue) together with those of the flavin S_1 state and the bleach (green and gray, respectively). Result of a global biexponential fit is shown in red, and decay times are indicated. (B) Concentrations of tryptophan neutral radical (blue) and tryptophan cation radical (green). (C) Concentration ratio between flavin anion radical and the sum of tryptophan radicals is shown in blue after 100 ps delay. Concentration ratio between tryptophan cation radical and tryptophan neutral radical is shown in green. Red lines show the average calculated after 100 ps delay. Note that concentrations on the sub-100 ps time scale may be somehow biased by cooling-induced spectral diffusion.

behavior has been previously observed at later times as is deduced from the biphasic decay of the flavin neutral radical in CPH1-PHR[23] and AtCRY1.[24] The following picture emerges: (i) early (~1 ps) spectra show already significant contributions of electronically excited oxidized flavin, flavin anion radical, and tryptophan radicals, which confirms that intraprotein electron transfer is behind femtosecond spectral evolution; (ii) 60−80% of the initially excited flavin undergoes electron transfer; (iii) relative concentrations appear to evolve on the 100 ps time scale only. Concentration ratios stay constant after 100 ps, meaning that a quasi-stationary state has been reached by that time.

The time evolution of the concentrations was fitted globally with a biexponential function. The resulting lifetimes are τ_1 = 31 ps and $\tau_2 \approx$ 1.4 ns. τ_1 seems to characterize a complex process in which the concentration of flavin anion radical still increases while that of excited flavin decreases (Figure 7A). Decay of $[WH^{\bullet +}]$ and rise of $[W^{\bullet}]$ occur concomitantly (Figure 7B). τ_2 characterizes the decay of all populations in the quasi-stationary state. This indicates that radical pair recombination and S_1 decay take place to some (minor) extent in this time scale. However, this issue will not be further discussed because it is not well determined in our experiment. We only stress that, for long delays, the ratios $[WH^{\bullet +}]/[W^{\bullet}]$ and $([FH^{\bullet -}])/([W^{\bullet}] + [WH^{\bullet +}])$ scatter around mean values of 1.3 and 0.99, respectively. The latter value strongly suggests that tryptophan is the only electron donor in this time regime. The ratio $[WH^{\bullet +}]/[W^{\bullet}]$ is 2−3 times higher than that deduced from the initial spectrum in the late nanosecond measurements[23] and deserves some comment. If one assumes a dissociation process $WH^{\bullet +} \rightarrow W^{\bullet} + H^{+}$ with rate constant k, the ratio $[WH^{\bullet +}]/[W^{\bullet}]$ approaches $([WH^{\bullet +}]_0/[W^{\bullet}]_0) \times (1 - kt)$ for sufficiently short times. Therefore, a decrease of 30−50% in the ratio $[WH^{\bullet +}]/[W^{\bullet}]$ on a time window of ~100 ns translates into a rate constant $k \approx 5-7 \times 10^6$ s^{-1}. This is the expected deprotonation rate constant for a weak acid ($pK_a \approx 4$) in water solution.[38] Therefore, the discrepancy between the values $[WH^{\bullet +}]/[W^{\bullet}]$ in the femtosecond and nanosecond experiments is consistent with deprotonation of tryptophan cation

dx.doi.org/10.1021/ja302121z | J. Am. Chem. Soc. 2012, 134, 12536−12546

radical to the bulk. We remind that no evidence of a tryptophan cation radical could be found in the microsecond time range.[23] Altogether, indication for an additional slow dissociation of the tryptophan cation radical to the solvent on the nanosecond to microsecond time scale is obtained. This was the only deprotonation process observed for DNA photolyase.[38]

Turning back to the exponential behavior characterized by τ_1, it is arguable if it monitors only changes in concentration. First, the concentration ratio between $FH^{\bullet -}$ and the tryptophan radicals ($WH^{\bullet +}$ and $W^{\bullet}$) increases from ~0.7 at time zero to ~1 at 100 ps. If this corresponded to true population dynamics, the excess concentration of tryptophan radicals would imply an additional electron acceptor X that is reduced by tryptophan just after flavin excitation. The anion radical of the hypothetical species $X^{\cdot -}$ would (a) not absorb in our spectral window and (b) reduce back the flavin simultaneous to the equilibration of tryptophan cation and neutral radical. This scenario is unlikely. Second, the fitting procedure assumes that the spectra of flavin and tryptophan radicals remain constant during the earliest 100 ps. However, this is improbable because radical ions are expected to be formed vibrationally hot. Vibrational cooling of riboflavin in DMSO occurs faster than τ_1 = 31 ps. A 4 ps time constant was reported by Wolf et al.[57] Similarly, cooling time constants ranging from from 2[58,59] to 10 ps[60] have been reported for different proteins (see Supporting Information). However, slower bimodal behavior was also reported. Ultrafast Raman[61] and IR[62] measurements provided direct evidence of bimodal vibrational cooling in heme proteins with time constants in the range of 2−9 and ~15−25 ps. Constants of 15−25 ps are consistent with heat diffusion from the chromophore through the protein to the surrounding solvent.[62] Remarkably, the latter ultrafast Raman[61] and IR[62] measurements monitor the cooling process directly. Computer simulations by Henry et al.[63] provide further support: 1−4 (50%) and 20−40 ps.

Thus, consistent with the time constants found by multiexponential fits and spectral decomposition, vibrational cooling is expected to proceed in the sub 100 ps time scale. It gives rise to transient spectra that blue shift and narrow with constant area.[64,65] In fact, the empirical finding that $[WH^{\bullet +}]$ decreases while $[W^{\bullet}]$ increases on the 100 ps time scale is qualitatively consistent with vibrational cooling: rise of $[W^{\bullet}]$ and decay of $[WH^{\bullet +}]$ translates into a spectral blue shift around 550 nm.

We conclude that vibrational cooling is most probably the reason behind some of the spectral evolution on the 100 ps time frame. This interpretation has to be validated further by femtosecond Raman[61] and IR[62] measurements specifically designed to follow vibrational cooling in the course of cryptochrome photodynamics. We underline that this does not rule out population evolution due to electron migration and proton-transfer processes occurring concomitantly to (or being controlled by) vibrational cooling. Time evolution of the anisotropy provides corroborating evidence for the electron- and proton-transfer processes concomitant to vibrational cooling (see below).

Picosecond Proton Transfer from Tryptophan. Picosecond proton transfer of $WH^{\bullet +}$ in plant cryptochrome contrasts with the much slower deprotonation time of 300 ns determined in DNA photolyase. The latter is consistent with deprotonation of a weak acid ($pK_a \approx 4$) to bulk water.[38,66,67] Consequently, deprotonation of WH^{+} in plant cryptochrome must be accelerated through a pre-established hydrogen bond with a *more* basic species. Only a few basic amino acids need to be considered: histidine, cysteine, tyrosine, lysine, and arginine. They show side chain pK_a values of 6.04, 8.10, 10.10, 10.67, and 12.10, respectively.[68] However, most of these basic side-chains will already be protonated at experimental pH (7.5) if exposed to the solvent. Histidine is the only exception. With a pK_a for side chain deprotonation of 6.04, histidine has a basic imidazole nitrogen available at physiological pH. The pK_a difference between histidine and tryptophan cation radical $\Delta pK_a = pK_a^{His} - pK_a^{WH^+} \approx 2$ is high enough to enable fast proton transfer if both units are hydrogen bonded, either directly or via a water bridge. Remarkably, the PHR domain of *At*CRY1 shows a high density of histidine residues around the tryptophan triad. H52, H307, H31,1 and H318 surround W377 at a 7−11 Å edge-to-edge distance (Scheme 1). H318 is 8 Å away from the terminal tryptophan W324, and W379 sits 8 Å away from H52. In CPH1, H311 and H318 are conserved as H308 and H315 whereas H52 is replaced by H380 and H326 at similar distances in the model. While the edge-to-edge distances are too long for a hydrogen bond, all these histidines in *At*CRY1 are accommodated in flexible loops facing the protein surface and exposed to the solvent. The probability of finding at least one histidine at proton-transfer distances or connected by a water bridge to the terminal tryptophan(s) should not be negligible. In support of this idea, structural analysis of different photolyases[69−72] shows that the high density of flexible histidines close to the terminal tryptophans of the triad is a characteristic of *At*CRY1. For instance, in *Drosophila* (6−4) photolyase only two α-helical histidines (H333 and H336) are found 12 Å apart from terminal W330.[71] In *Thermus thermophilus* CPD photolyase, a single α-helical histidine (H323) is in the neighborhood (10 Å) of the end tryptophan W275.[70] Most remarkably, no histidine is found in the surroundings of the terminal tryptophan W306 of CPD photolyase from *E. coli* (PDB Code 1DNP),[69] where the proton-transfer time constant (300 ns) is consistent with weak acid dissociation to bulk solvent.[38] Only H294 sits 6 Å away from W359, the middle tryptophan of the triad.

For other cryptochromes besides plant cryptochromes, the ultrafast triad reaction has only been characterized for *Ot*CPF1 and *Ot*CPF2 but did not show any indication for a picosecond

Scheme 1. Histidines (H) Surrounding the Middle and Terminal Tryptophans (W) in the Triad of *At*CRY1[a]

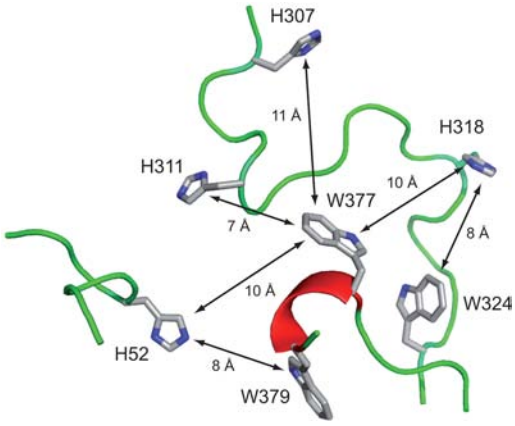

[a]The histidines sit in flexible loops and may act as proton acceptors for ultrafast deprotonation of the tryptophan cation radical (PDB 1U3C).[22]

dx.doi.org/10.1021/ja302121z | J. Am. Chem. Soc. 2012, 134, 12536−12546

deprotonation of the tryptophan radical.[36] For *Ot*CPF1, modeling on a (6−4) photolyase structure suggests that a single, helical histidine is present in hydrogen-bonding distance to the middle tryptophan, whereas in a model of *Ot*CPF2 on a DASH cryptochrome three histidines, again all helical, may be present at a 9−10 Å distance. Thus, we propose that the local high concentration of flexible histidines around the middle and terminal tryptophan(s) in plant cryptochromes explains fast deprotonation of the cation radical. Further experiments on other cryptochromes are necessary to determine whether the ultrafast tryptophan deprotonation is specific for plant cryptochromes only.

Analysis of the Anisotropy. We close this section with the analysis of the time-dependent anisotropy. Figure 3 shows the evolution of the anisotropy at four representative wavelengths: 370, 455, 500, and 545 nm. Three independent experiments were overlaid for each wavelength. The analyzed wavelengths are also indicated in the spectral decomposition of Figure 6. We address first the anisotropy at 455 and 370 nm. Only flavin bleach contributes at 455 nm, while flavin $S_1 \rightarrow S_n$ and flavin anion radical $S_0 \rightarrow S_n$ absorption are the dominating transitions at 370 nm. Constant anisotropy at both wavelengths demonstrates that (a) rotational diffusion of the protein is orders of magnitude slower than 1 ns and (b) these particular transitions are not affected by the electron- and proton-transfer reactions discussed above. On the other hand, time evolution of the anisotropy at 500 and 545 nm monitors the rise and decay of species involved in the electron- and proton-transfer processes (Figure 6). Thus, the anisotropy evolves exponentially with a 0.3 ± 0.2 ps time constant at 500 nm, where flavin $S_1 \rightarrow S_{n-1}$ ESA decays and absorption by tryptophan radicals rises (Figure 6). In turn, the FAD S_1 absorption/SE is close to zero at 545 nm. Therefore, the anisotropy mainly monitors the build up of Trp radicals with a small background absorption of flavin anion radical (Figure 6). The time evolution of the anisotropy is bimodal at this wavelength: 4 ± 2 (75%) and 130 ± 40 ps. An average time constant can be calculated as $\tau_{avg} = a_1\tau_1 + a_2\tau_2 = 36$ ps. The latter matches the time constant τ_1 obtained by spectral decomposition which was already assigned to vibrational cooling. Thus, the direction of the transition dipoles associated to tryptophan radical evolves on the same time scale as vibrational cooling. However, vibrational cooling cannot explain the changes in the anisotropy. Either reorganization of the primary electron donor (W_{400}) or migration of the positive hole from the pocket to the surface must be postulated. Only the latter scenario is consistent with site-directed mutagenesis experiments by Lukacs et al.[39] and EPR measurements by Biskup et al.[73] in DNA photolyase and DASH cryptochrome, respectively. Altogether, evidence of surface-to-pocket charge migration has been obtained. The process proceeds within the time scale of vibrational cooling.

Limit values of the anisotropy provide further support. The anisotropy reaches a value of ∼0 in the limit of long delays at 545 nm. This implies that the dipole transition moment associated to the optical transitions extending from 500 to ∼600 nm forms an angle of ∼55° with the flavin $S_1 \rightarrow S_0$ transition moment. It was deduced from the analysis above that $W^{\bullet}$ and $WH^{\bullet+}$ are the only species absorbing in this range at long delays. In other words, the limit value of the anisotropy provides the relative orientation of the flavin and the tryptophan radicals surviving after 100 ps. Any candidate has to fulfill this requirement.

The structure of *At*CRY[22] was analyzed to extract the relative orientations of the tryptophans around the flavin cofactor. It was assumed that the $S_1 \rightarrow S_0$ transition moment of the flavin cofactor is oriented along the C_8-N_3 axis,[74] while for both tryptophan radicals the direction of the transition dipole moment of the first electronic transition was approximated as C_7-C_2[75] (see Scheme 2 for atom numbering). The resulting angles between the transition dipoles of both species are 45° for W400, 22° for W377, 50° for W379, and 72° for W324. Thus, W400 and W379 exhibit angles comparable to the experimental result. Mutational studies on *At*CRY1 have shown that W324 is a likely candidate for the terminal tryptophan, but W379 has not been investigated yet.[20] An additional piece of information comes from time-resolved EPR experiments performed on a DASH cryptochrome and its W324F mutant.[73] These experiments have shown that an inter-radical distance of 20 Å is necessary to model the EPR signal. The current analysis relies on the structural homology between *At*CRY1 and CPH1. Although W324 cannot be completely excluded as the electron donor, both relative orientation (50°) and distance (∼15 Å) point here to W379 as the ultimate donor.

Scheme 2. Numbering of Atoms in Flavin and Tryptophan

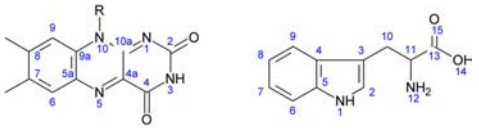

CONCLUSIONS

Early stages of signaling state formation in the plant cryptochrome CPH1 were studied by femtosecond transient absorption (Scheme 3). Intraprotein electron transfer to the flavin was observed with a 0.4 ps time constant. The resulting flavin anion radical remains for 7 orders of magnitude in time scale until the neutral radical is formed by proton transfer.[23] Hole migration to a tryptophan on the protein surface is completed by 100 ps delay, most likely to W379 (in *At*CRY1 numbering) as deduced from anisotropy analysis. In the same time frame, partial proton transfer from the tryptophan radical cation to the nearest environment takes place. Therefore, an

Scheme 3. Mechanism for Signaling State Formation in the Plant Cryptochrome CPH1[a]

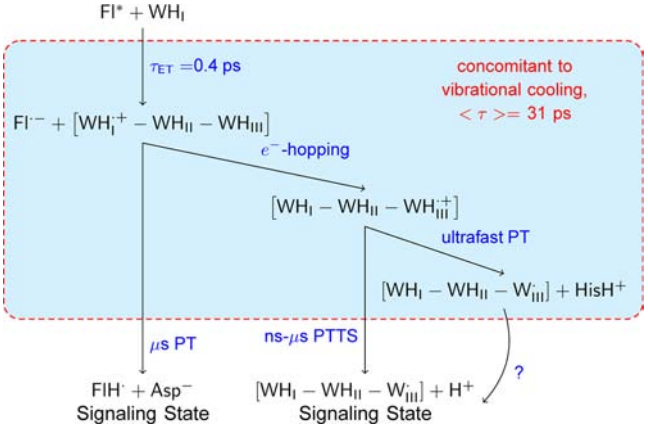

[a] W_I refers to W_{400}, W_{II} to W_{377}, and W_{III} to W_{324} and/or W_{379}.

dx.doi.org/10.1021/ja302121z | J. Am. Chem. Soc. 2012, 134, 12536−12546

additional proton-transfer channel was observed in plant cryptochrome ($k_{PT} \approx 10$ ns^{-1}) as compared to CPD photolyases ($k_{PT} \approx 3 \times 10^{-3}$ ns^{-1}) despite their high structural homology. Structural comparison suggests that the difference lies in several histidines sitting on flexible loops around the terminal tryptophans in plant cryptochrome which might act as proton acceptors. This rapid proton transfer prevents charge recombination and favors stabilization of the radical pair. Magnetic field effects on the yield of radical pair formation in plant cryptochromes have recently been demonstrated.[76] It needs to be investigated whether ultrafast stabilization of the radical pair takes place in animal cryptochromes as well and might play a role for magnetoreception. The reversibility of electron-transfer reactions poses a general challenge in stabilization of a radical pair against charge recombination. Plant cryptochromes exhibit at least three separate mechanisms of stabilization. Separation in space to ∼15 Å distance via a tryptophan triad decelerates electron back transfer. Rapid picosecond to nanosecond deprotonation of $WH^{\bullet+}$ as well as microsecond protonation of flavin anion radical lead to the much more stable pair ($W^{\bullet}\cdots FlH^{\bullet}$). Only the combination of these effects ensures a millisecond lifetime[77] for signal transfer to the C-terminal domain.

■ ASSOCIATED CONTENT

Supporting Information

Notes on theory of anisotropy signal in femtosecond transient absorption, basis set for spectral decomposition of picosecond transient absorption, and global fits of band integrals. This material is available free of charge via the Internet at http://pubs.acs.org.

■ AUTHOR INFORMATION

Corresponding Author

E-mail: tilman.kottke@uni-bielefeld.de; luis.lustres@usc.es

Notes

The authors declare no competing financial interest.

■ ACKNOWLEDGMENTS

The authors thank the Deutsche Forschungsgemeinschaft (DFG) for financial support via the UniCat Cluster of Excellence and the FOR-526. J.L.P.L. thanks the Spanish Ministry of Science and Innovation (MICINN) for funding through grant CTQ2010-17026 (FEDER Funds) and the Ramón y Cajal Programm 2009. A.W. further acknowledges support from a Kekulé grant of the Fonds der Chemischen Industrie. Joachim Heberle and Niko Ernsting are acknowledged for generous support.

■ REFERENCES

(1) Stanewsky, R.; Kaneko, M.; Emery, P.; Beretta, B.; Wager-Smith, K.; Kay, S.; Rosbash, M.; Hall, J. *Cell* **1998**, *95*, 681−692.

(2) Somers, D. E.; Devlin, P. F.; Kay, S. A. *Science* **1998**, *282*, 1488−1490.

(3) Lin, C.; Shalitin, D. *Annu. Rev. Plant Biol.* **2003**, *54*, 469−496.

(4) Coesel, S.; Mangogna, M.; Ishikawa, T.; Heijde, M.; Rogato, A.; Finazzi, G.; Todo, T.; Bowler, C.; Falciatore, A. *EMBO Rep.* **2009**, *10*, 655−661.

(5) Hendrischk, A. K.; Frühwirth, S. W.; Moldt, J.; Pokorny, R.; Metz, S.; Kaiser, G.; Jäger, A.; Batschauer, A.; Klug, G. *Mol. Microbiol.* **2009**, *74*, 990−1003.

(6) Fogle, K. J.; Parson, K. G.; Dahm, N. A.; Holmes, T. C. *Science* **2011**, *331*, 1409−1413.

(7) Gegear, R. J.; Casselman, A.; Waddell, S.; Reppert, S. M. *Nature* **2008**, *454*, 1014−U61.

(8) Ritz, T.; Adem, S.; Schulten, K. *Biophys. J.* **2000**, *78*, 707−718.

(9) Mouritsen, H.; Ritz, T. *Curr. Opin. Neurobiol.* **2005**, *15*, 406−414.

(10) Griffin, E. A.; Staknis, D.; Weitz, C. J. *Science* **1999**, *286*, 768−771.

(11) Zhu, H.; Sauman, I.; Yuan, Q.; Casselman, A.; Emery-Le, M.; Emery, P.; Reppert, S. M. *PLoS Biol.* **2008**, *6*, 138−155.

(12) Selby, C. P.; Sancar, A. *Proc. Natl. Acad. Sci. U.S.A.* **2006**, *103*, 17696−17700.

(13) Pokorny, R.; Klar, T.; Hennecke, U.; Carell, T.; Batschauer, A.; Essen, L. O. *Proc. Natl. Acad. Sci. U.S.A.* **2008**, *105*, 21023−21027.

(14) Sancar, A. *Chem. Rev.* **2003**, *103*, 2203−2237.

(15) Losi, A. *Photochem. Photobiol.* **2007**, *83*, 1283−1300.

(16) Lin, C. T.; Robertson, D. E.; Ahmad, M.; Raibekas, A. A.; Jorns, M. S.; Dutton, P. L.; Cashmore, A. R. *Science* **1995**, *269*, 968−970.

(17) Yang, H.; Wu, Y.; Tang, R.; Liu, D.; Liu, Y.; Cashmore, A. *Cell* **2000**, *103*, 815−827.

(18) Bouly, J.-P.; Schleicher, E.; Dionisio-Sese, M.; Vandenbussche, F.; Van Der Straeten, D.; Bakrim, N.; Meier, S.; Batschauer, A.; Galland, P.; Bittl, R.; Ahmad, M. *J. Biol. Chem.* **2007**, *282*, 9383−9391.

(19) Banerjee, R.; Schleicher, E.; Meier, S.; Viana, R. M.; Pokorny, R.; Ahmad, M.; Bittl, R.; Batschauer, A. *J. Biol. Chem.* **2007**, *282*, 14916−14922.

(20) Zeugner, A.; Byrdin, M.; Bouly, J.; Bakrim, N.; Giovani, B.; Brettel, K.; Ahmad, M. *J. Biol. Chem.* **2005**, *280*, 19437−19440.

(21) Li, X.; Wang, Q.; Yu, X.; Liu, H.; Yang, H.; Zhao, C.; Liu, X.; Tan, C.; Klejnot, J.; Zhong, D.; Lin, C. *Proc. Natl. Acad. Sci. U.S.A.* **2011**, *108*, 20844−20849.

(22) Brautigam, C. A.; Smith, B. S.; Ma, Z. Q.; Palnitkar, M.; Tomchick, D. R.; Machius, M.; Deisenhofer, J. *Proc. Natl. Acad. Sci. U.S.A.* **2004**, *101*, 12142−12147.

(23) Langenbacher, T.; Immeln, D.; Dick, B.; Kottke, T. *J. Am. Chem. Soc.* **2009**, *131*, 14274−14280.

(24) Giovani, B.; Byrdin, M.; Ahmad, M.; Brettel, K. *Nat. Struct. Biol.* **2003**, *10*, 489−490.

(25) Kottke, T.; Batschauer, A.; Ahmad, M.; Heberle, J. *Biochemistry* **2006**, *45*, 2472−2479.

(26) Immeln, D.; Pokorny, R.; Herman, E.; Moldt, J.; Batschauer, A.; Kottke, T. *J. Phys. Chem. B* **2010**, *114*, 17155−17161.

(27) Balland, V.; Byrdin, M.; Eker, A. P. M.; Ahmad, M.; Brettel, K. *J. Am. Chem. Soc.* **2009**, *131*, 426−427.

(28) Berndt, A.; Kottke, T.; Breitkreuz, H.; Dvorsky, R.; Hennig, S.; Alexander, M.; Wolf, E. *J. Biol. Chem.* **2007**, *282*, 13011−13021.

(29) Song, S.-H.; Ozturk, N.; Denaro, T. R.; Arat, N. O.; Kao, Y.-T.; Zhu, H.; Zhong, D.; Reppert, S. M.; Sancar, A. *J. Biol. Chem.* **2007**, *282*, 17608−17612.

(30) Ozturk, N.; Selby, C. P.; Annayev, Y.; Zhong, D.; Sancar, A. *Proc. Natl. Acad. Sci. U.S.A.* **2011**, *108*, 516−521.

(31) Mataga, N.; Chosrowjan, H.; Shibata, Y.; Tanaka, F.; Nishina, Y.; Shiga, K. *J. Phys. Chem. B* **2000**, *104*, 10667−10677.

(32) Zhong, D.; Zewail, A. *Proc. Natl. Acad. Sci. U.S.A.* **2001**, *98*, 11867−11872.

(33) Kao, Y. T.; Saxena, C.; He, T. F.; Guo, L. J.; Wang, L. J.; Sancar, A.; Zhong, D. P. *J. Am. Chem. Soc.* **2008**, *130*, 13132−13139.

(34) Gauden, M.; van Sotokkum, I. H. M.; Key, J. M.; Lührs, D. C.; van Grondelle, R.; Hegemann, P.; Kennis, J. T. *Proc. Natl. Acad. Sci. U.S.A.* **2006**, *103*, 10895−10900.

(35) Shirdel, J.; Zirak, P.; Penzkofer, A.; Breitkreuz, H.; Wolf, E. *Chem. Phys.* **2008**, *352*, 35−47.

(36) Brazard, J.; Usman, A.; Lacombat, F.; Ley, C.; Martin, M. M.; Plaza, P.; Mony, L.; Heijde, M.; Zabulon, G.; Bowler, C. *J. Am. Chem. Soc.* **2010**, *132*, 4935−4945.

(37) Brettel, K.; Byrdin, M. *Curr. Opin. Struct. Biol.* **2010**, *20*, 693−701.

(38) Aubert, C.; Vos, M. H.; Mathis, P.; Eker, A. P. M.; Brettel, K. *Nature* **2000**, *405*, 586−590.

(39) Lukacs, A.; Eker, A. P. M.; Byrdin, M.; Brettel, K.; Vos, M. H. *J. Am. Chem. Soc.* **2008**, *130*, 14394−14395.

(40) Immeln, D.; Schlesinger, R.; Heberle, J.; Kottke, T. *J. Biol. Chem.* **2007**, *282*, 21720−21728.
(41) Kovalenko, S. A.; Dobryakov, A. L.; Ruthmann, J.; Ernsting, N. P. *Phys. Rev. A* **1999**, *59*, 2369−2384.
(42) Dobryakov, A. L.; Kovalenko, S. A.; Weigel, A.; Perez-Lustres, J. L.; Lange, J.; Mueller, A.; Ernsting, N. P. *Rev. Sci. Instrum.* **2010**, *81*, 113106.
(43) Weigel, A.; Dobryakov, A. L.; Veiga, M.; Lustres, J. L. P. *J. Phys. Chem. A* **2008**, *112*, 12054−12065.
(44) Weigel, A.; Dobryakov, A.; Klaumuenzer, B.; Sajadi, M.; Saalfrank, P.; Ernsting, N. P. *J. Phys. Chem. B* **2011**, *115*, 3656−3680.
(45) Land, E. J.; Swallow, A. J. *Biochemistry* **1969**, *8*, 2117−2125.
(46) Hanine-Lmoumene, C. E.; Lindqvist, L. *Photochem. Photobiol.* **1997**, *66*, 591−595.
(47) Kottke, T.; Heberle, J.; Hehn, D.; Dick, B.; Hegemann, P. *Biophys. J.* **2003**, *84*, 1192−1201.
(48) Grodowski, M.; Veyret, B.; Weiss, K. *Photochem. Photobiol.* **1977**, *26*, 341−352.
(49) Solar, S.; Getoff, N.; Surdhar, P. S.; Armstrong, D. A.; Singh, A. *J. Phys. Chem.* **1991**, *95*, 3639−3643.
(50) Das, T. N. *J. Phys. Chem. A* **2005**, *109*, 3344−3351.
(51) Glas, A. F.; Maul, M. J.; Cryle, M.; Barends, T. R. M.; Schneider, S.; Kaya, E.; Schlichting, I.; Carell, T. *Proc. Natl. Acad. Sci. U.S.A.* **2009**, *106*, 11540−11545.
(52) Klar, T.; Pokorny, R.; Moldt, J.; Batschauer, A.; Essen, L. O. *J. Mol. Biol.* **2007**, *366*, 954−964.
(53) Chosrowjan, H.; Taniguchi, S.; Mataga, N.; Tanaka, F.; Visser, A. *Chem. Phys. Lett.* **2003**, *378*, 354−358.
(54) Kao, Y. T.; Tan, C.; Song, S. H.; Ozturk, N.; Li, J.; Wang, L. J.; Sancar, A.; Zhong, D. P. *J. Am. Chem. Soc.* **2008**, *130*, 7695−7701.
(55) Tanaka, F.; Chosrowjan, H.; Taniguchi, S.; Mataga, N.; Sato, K.; Nishina, Y.; Shiga, K. *J. Phys. Chem. B* **2007**, *111*, 5694−5699.
(56) Tanaka, F.; Rujkorakarn, R.; Chosrowjan, H.; Taniguchi, S.; Mataga, N. *Chem. Phys.* **2008**, *348*, 237−241.
(57) Wolf, M. M. N.; Schumann, C.; Gross, R.; Domratcheva, T.; Diller, R. *J. Phys. Chem. B* **2008**, *112*, 13424−13432.
(58) Nagasawa, Y.; Fujita, K.; Katayama, T.; Ishibashi, Y.; Miyasaka, H.; Takabe, T.; Nagao, S.; Hirota, S. *Phys. Chem. Chem. Phys.* **2010**, *12*, 6067−6075.
(59) Diller, R.; Maiti, S.; Walker, G. C.; Cowen, B. R.; Pippenger, R.; Bogomolni, R. A.; Hochstrasser, R. M. *Chem. Phys. Lett.* **1995**, *241*, 109−115.
(60) Stoner-Ma, D.; Jaye, A. A.; Ronayne, K. L.; Nappa, J.; Meech, S. R.; Tonge, P. J. *J. Am. Chem. Soc.* **2008**, *130*, 1227−1235.
(61) Mizutani, Y.; Kitagawa, T. *Science* **1997**, *278*, 443−446.
(62) Lian, T.; Locke, B.; Kholodenko, Y.; Hochstrasser, R. *J. Phys. Chem.* **1994**, *98*, 11648−11656.
(63) Henry, E. R.; Eaton, W. A.; Hochstrasser, R. M. *Proc. Natl. Acad. Sci. U.S.A.* **1986**, *83*, 8982−8986.
(64) Kovalenko, S.; Schanz, R.; Farztdinov, V.; Hennig, H.; Ernsting, N. *Chem. Phys. Lett.* **2000**, *323*, 312−322.
(65) Kovalenko, S.; Schanz, R.; Hennig, H.; Ernsting, N. *J. Chem. Phys.* **2001**, *115*, 3256−3273.
(66) McGimpsey, W. G.; Görner, H. *Photochem. Photobiol.* **1996**, *64*, 501−509.
(67) Burdi, D.; Aveline, B. M.; Wood, P. D.; Stubbe, J.; W., R. R. *J. Am. Chem. Soc.* **1997**, *119*, 6457−6460.
(68) In *Handbook of Chemistry and Physics*, 84th ed.; Lide, D. R., Ed.; CRC Press: Boca Raton, FL, 2003−2004.
(69) Park, H. W.; Kim, S. T.; Sancar, A.; Deisenhofer, J. *Science* **1995**, *268*, 1866−1872.
(70) Komori, H.; Masui, R.; Kuramitsu, S.; Yokoyama, S.; Shibata, T.; Inoue, Y.; Miki, K. *Proc. Natl. Acad. Sci. U.S.A.* **2001**, *98*, 13560−13565.
(71) Maul, M. J.; Barends, T. R. M.; Glas, A. F.; Cryle, M. J.; Domratcheva, T.; Schneider, S.; Schlichting, I.; Carell, T. *Angew. Chem., Int. Ed.* **2008**, *47*, 10076−10080.
(72) Hitomi, K.; DiTacchio, L.; Arvai, A. S.; Yamamoto, J.; Kim, S. T.; Todo, T.; Tainer, J. A.; Iwai, S.; Panda, S.; Getzoff, E. D. *Proc. Natl. Acad. Sci. U.S.A.* **2009**, *106*, 6962−6967.
(73) Biskup, T.; Schleicher, E.; Okafuji, A.; Link, G.; Hitomi, K.; Getzoff, E. D.; Weber, S. *Angew. Chem., Int. Ed.* **2009**, *48*, 404−407.
(74) Climent, T.; González-Luque, R.; Merchán, M.; Serrano-Andrés, L. *J. Phys. Chem. A* **2006**, *110*, 13584−13590.
(75) Byrdin, M.; Villette, S.; Espagne, A.; Eker, A. P. M.; Brettel, K. *J. Phys. Chem. B* **2008**, *112*, 6866−6871.
(76) Maeda, K.; Robinson, A. J.; Henbest, K. B.; Hogben, H. J.; Biskup, T.; Ahmad, M.; Schleicher, E.; Weber, S.; Timmel, C. R.; Hore, P. J. *Proc. Natl. Acad. Sci. U.S.A.* **2012**, *109*, 4774−4779.
(77) Kondoh, M.; Shiraishi, C.; Müller, P.; Ahmad, M.; Hitomi, K.; Getzoff, E. D.; Terazima, M. *J. Mol. Biol.* **2011**, *413*, 128−137.